Int. J. Therm. Sci. (2001) 40, 152–164

S1290-0729(00)01204-7/FLA

Gas flow and heat transfer through catalyst filled tubes

Oliver Bey [a], Gerhart Eigenberger [b]*

[a] *BASF AG, 67056 Ludwigshafen, Germany*

[b] *Universität Stuttgart, Institut für Chemische Verfahrenstechnik, Böblinger Str. 72, 70199 Stuttgart, Germany*

(Received 5 November 1999, accepted 16 March 2000)

Abstract — A detailed knowledge of the fluid flow profile and of the radial heat transfer parameters is essential for a proper design of fixed-bed processes. For different sphere, ring and cylinder catalysts radial velocity profiles were measured below the fixed-bed at empty tube velocities of air between $0.5\ \mathrm{m{\cdot}s^{-1}} < v_0 < 1.5\ \mathrm{m{\cdot}s^{-1}}$ and tube to particle diameter ratios $3.3 < d_t/d_P < 11$. As a consequence of the statistical behaviour of packings, it was necessary to average velocity measurements after repacking in order to obtain representative flow profiles. All profiles show a velocity maximum in the vicinity of the wall. In order to relate the measured profiles below the packing to the velocity profiles inside the packing, model simulations have been performed. The model is based on the extended Brinkman equation and the independently determined radial void fraction profiles. It considers an "effective viscosity" for which correlations have been derived for spheres, cylinders and rings. Radial heat transfer parameters were obtained experimentally from packings between two parallel plates of different temperatures. The determined heat transfer parameters can be transformed to the round cross section of a tube by considering the respective radial velocity profiles. The transformed values of the effective heat conductivity could be well described by literature correlations. For the heat transfer coefficient at the wall a new correlation was developed. © 2001 Éditions scientifiques et médicales Elsevier SAS

fixed bed reactor / modeling / fluid flow / bypass behaviour / effective viscosity / heat transfer / effective radial (heat) conductivity / wall heat transfer coefficient / radial flow distribution / fixed-bed adsorption

Nomenclature

a_{spec}	specific surface of full particle	$\mathrm{m^2{\cdot}m^{-3}}$
Bi_0	Biot number, equation (14)	
$c_{p,f}$	specific fluid heat capacity	$\mathrm{J{\cdot}kg^{-1}{\cdot}K^{-1}}$
d_a	outer diameter of a cylinder or ring particle	m
d_e	equivalent sphere diameter $= 6V_P/A_P$	m
$d_{e,HC}$	equivalent sphere diameter for rings after Brauer, equation (34)	m
d_i	inner diameter of a ring particle	m
d_P	particle diameter	m
d_{PS}	equivalent sphere diameter without inner voidage	m
d_t	tube diameter	m
E^n	factor to consider the inner void fraction of a ring used in the correlation for the pressure drop in a packing of rings	
K_r	constant to correlate the effective heat conductivity	
$K_{r,t}$	constant to correlate the effective heat conductivity in the tube	
l_P	particle length	m
l_t	length of the heated section	m
$\dot{m}_{z,0}$	specific mass flow in the empty tube in axial direction	$\mathrm{kg{\cdot}m^{-2}{\cdot}s^{-1}}$
Nu_W	Nusselt number $= \alpha_W d_P/\lambda_f$	
$Nu_{W,0}$	Nusselt number at stagnant flow conditions	
p	pressure	Pa
Pe_P	particle Péclet number $= v_0 d_P \rho_f c_{p,f}/\lambda_f$	
$\dot{q}_W$	specific heat flux	$\mathrm{W{\cdot}m^{-2}}$
R	tube radius	m
r	radial coordinate	m
r'	dimensionless radial coordinate	
Re_P	particle Reynolds number $= v_0 \rho_f d_P/\eta_f$	
s	duct width (distance between parallel plates)	m
T	temperature	K
T_{in}	entrance temperature	K
T_W	wall temperature	K
v	interstitial velocity	$\mathrm{m{\cdot}s^{-1}}$
$v_{0,max}$	maximum empty tube velocity	$\mathrm{m{\cdot}s^{-1}}$

* Correspondence and reprints.
E-mail address: egb@icvt.uni-stuttgart.de (G. Eigenberger).

v_0	average empty tube flow velocity, $\lvert v_0\rvert = \sqrt{v_{z,0}^2 + v_{r,0}^2}$	$\mathrm{m{\cdot}s^{-1}}$
$v_{0,z}$	average empty tube flow velocity in axial direction	$\mathrm{m{\cdot}s^{-1}}$
v_z	axial interstitial velocity	$\mathrm{m{\cdot}s^{-1}}$
x	lateral coordinate	m
x^+	dimensionless axial coordinate in the monolith	
$x_{\min}$	distance between tube wall and the contact point of two spheres touching the tube wall	m
z	axial coordinate	m

Greek symbols

α_W	heat transfer coefficient at the tube wall of the packed bed	$\mathrm{W{\cdot}m^{-2}{\cdot}K^{-1}}$
ε	local void fraction	$\mathrm{m^3_{fluid}{\cdot}m^{-3}_{total}}$
$\overline{\varepsilon}$	mean void fraction	$\mathrm{m^3_{fluid}{\cdot}m^{-3}_{total}}$
ε_0	void fraction in the core of the packed bed	$\mathrm{m^3_{fluid}{\cdot}m^{-3}_{total}}$
$\varepsilon_{0,\mathrm{HC}}$	void fraction in the core of the packed bed of rings	$\mathrm{m^3_{fluid}{\cdot}m^{-3}_{total}}$
$\varepsilon_{0,\mathrm{C}}$	void fraction in the core of the packed bed of cylinders	$\mathrm{m^3_{fluid}{\cdot}m^{-3}_{total}}$
ε_i	inner void fraction of a ring $= d_\mathrm{i}^2/d_\mathrm{a}^2$	$\mathrm{m^3_{fluid}{\cdot}m^{-3}_{total}}$
$\varepsilon_{\min}$	minimum void fraction	$\mathrm{m^3_{fluid}{\cdot}m^{-3}_{total}}$
$\varepsilon_{\min,\mathrm{HC}}$	minimum void fraction in a packed bed of rings	$\mathrm{m^3_{fluid}{\cdot}m^{-3}_{total}}$
$\varepsilon_{\min,\mathrm{C}}$	minimum void fraction in a packed bed of cylinders	$\mathrm{m^3_{fluid}{\cdot}m^{-3}_{total}}$
$\overline{\varepsilon}_\mathrm{C}$	void fraction for the whole cross section of a cylinder packing	$\mathrm{m^3_{fluid}{\cdot}m^{-3}_{total}}$
$\overline{\varepsilon}_\mathrm{HC}$	void fraction for the whole cross section of a ring packing	$\mathrm{m^3_{fluid}{\cdot}m^{-3}_{total}}$
$\overline{\varepsilon}_\mathrm{S}$	void fraction for the whole cross section of a sphere packing	$\mathrm{m^3_{fluid}{\cdot}m^{-3}_{total}}$
η_eff	effective viscosity	$\mathrm{kg{\cdot}m^{-1}{\cdot}s^{-1}}$
η_f	dynamic viscosity	$\mathrm{kg{\cdot}m^{-1}{\cdot}s^{-1}}$
η_t	"turbulent" viscosity	$\mathrm{kg{\cdot}m^{-1}{\cdot}s^{-1}}$
λ_r	effective radial heat conductivity in the packed bed	$\mathrm{W{\cdot}m^{-1}{\cdot}K^{-1}}$
λ_z	effective axial heat conductivity in the packed bed	$\mathrm{W{\cdot}m^{-1}{\cdot}K^{-1}}$
ρ_f	density of the fluid	$\mathrm{kg{\cdot}m^{-3}}$

1. INTRODUCTION

Reactions which are characterized by a large heat evolution and a great temperature sensitivity are mostly carried out in wall cooled packed bed reactors. The behaviour of these reactors can be influenced by the reaction itself, by the radial heat and mass transfer perpendicular to the flow direction and by the radial mass flow profile which is a result of the nonuniform void fraction across the radius (Vortmeyer and Haidegger [1], Daszkowski and Eigenberger [2]). It is well known that in randomly packed beds the void fraction in the vicinity of the tube wall approaches unity. Therefore, fluid flow through the packed bed is characterized by a channeling effect at the wall. Nevertheless, most fixed bed reactor models used in industry are based on the assumption of plug flow and do not take into account radial maldistribution. Several research groups, in particular Vortmeyer [1], Papageorgiou and Froment [3] as well as Daszkowski and Eigenberger [2], questioned that reaction and radial heat transfer can be modeled correctly without properly considering radial inhomogeneities.

Despite of a fair number of publications, systematic investigations of the radial velocity profiles for small dimensionless tube diameters D/d_P are lacking, especially for nonspherical particles. Hence, the first subject of the following report is the systematic determination of radial velocity profiles in packings of spheres, cylinders and rings. As a result of these studies, correlations are given to evaluate fluid flow inside packed beds.

In the next section, these velocity profiles will be used in the determination of the radial effective heat transfer parameters, the wall heat transfer coefficient α_W and effective radial heat conductivity λ_r. Contrary to all previous data (see Tsotsas [4] and Dixon [5] for recent surveys), α_W and λ_r values have been obtained independently of each other by direct measurement in a parallel plate set-up.

2. GAS FLOW

The investigation of the radial velocity distribution was carried out in two steps. First the local velocities below packed beds were measured. A mathematical model was applied to reconstruct the velocity profile inside the packing.

Figure 1 shows a sketch of the experimental set-up. The position of the sensor can be varied in radial and in annular direction. To obtain the radial distribution, the measurements are averaged over each circumference. Details can be drawn from [6].

In *figure 2* velocity profiles after several repackings are plotted. The experiments show that the general bypass behaviour can be reproduced with an accuracy of ±20 %.

The velocities in the core region show much stronger scattering. This is an obvious consequence of the fact that no angular averaging can be performed at the centre of the tube. The differences between all measurements close to the wall represent the statistical behaviour of the fixed bed structure, which results in deviations of the radial voidage and velocity profile in axial direction (Borkin [7]). The mean velocity profile, representative of the whole bed, must, therefore, be obtained by averaging measured velocity profiles after repacking or by measuring inside the packing in different layers. So far no gas flow measurements inside of packed tubes have been reported and it remains uncertain whether the results of liquid flow measurements (Giese et al. [8]) can be used instead, because the behaviour might deviate due to the different compressibility.

Our gas flow measurements were, therefore, taken immediately below the fixed bed which was supported by a thin slice of a monolith. Before and behind the monolith the fluid shifts from the region near the wall to the centre. To take these changes into account, a two-dimensional model containing the continuity equation and the momentum balances in radial and axial direction is used. For the momentum balances the basic relations are the Navier–Stokes equations for the interstitial flow. They are extended by terms describing pressure drop in porous structures as a volume force. For full particles, for example, the correlation of Ergun is well established.

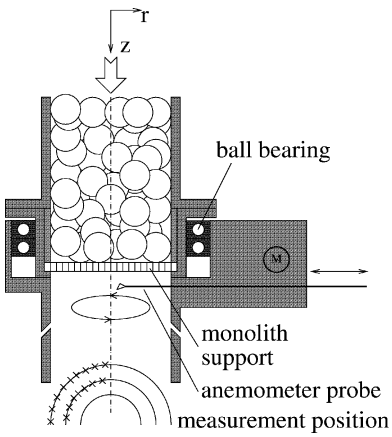

Figure 1. Sketch of the experimental setup for the measurement of $v(r)$.

Simulated flow distributions, based on void fraction profiles extracted from literature, are characterized by greater maximum velocities than measured flow profiles. An "effective turbulent viscosity" was therefore assumed and adjusted to such a value that the measured profiles below the bed could be matched [6]. The effective viscosity accounts for turbulent flow fluctuations inside a packing. It turns out that in our model the effective viscosity only plays a role in the larger voids at the tube wall. Its influence inside the packing has already been accounted for by the Ergun-type pressure drop relation.

The "effective" viscosities increase with increasing mean velocity v_0. Correlations of the effective viscosity as a function of particle Reynolds number have been derived and are given below.

A calculation of the radial velocity profile inside the packing can now be carried out with the extended Brinkman equation

$$\frac{\mathrm{d}p}{\mathrm{d}z} = -150\eta_\mathrm{f}\frac{(1-\varepsilon(r))^2}{\varepsilon(r)^2 d_\mathrm{e}^2}v(r) - 1.75\rho_\mathrm{f}\frac{1-\varepsilon(r)}{\varepsilon(r)d_\mathrm{e}}v(r)^2 + \frac{\eta_\mathrm{eff}}{\varepsilon(r)}\frac{1}{r}\frac{\mathrm{d}}{\mathrm{d}r}\left(\varepsilon(r)r\frac{\mathrm{d}v(r)}{\mathrm{d}r}\right) \quad (1)$$

together with the entrance equation

$$v_{0,z} = \frac{2}{R^2}\int_0^R v(r)\varepsilon(r)r\,\mathrm{d}r \quad (2)$$

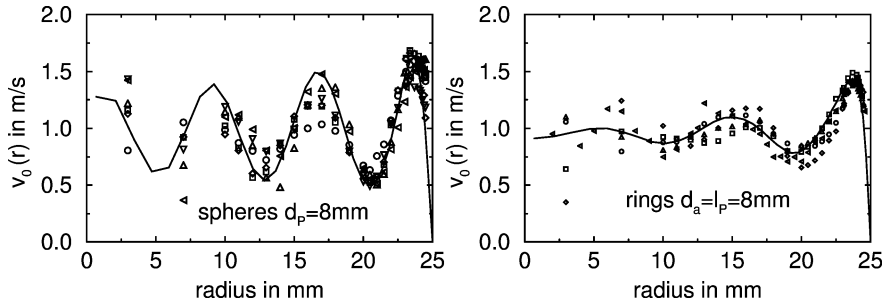

Figure 2. Comparison of measured velocity profiles $v(r)$ after repeated repacking, mean velocity $v_0 = 0.5$ m·s^{-1}. Lines represent the simulated flow profile.

and the correlations of the effective viscosities for *spheres*

$$\frac{\eta_{\mathrm{eff}}}{\eta_{\mathrm{f}}} = 1 + \left(7{\cdot}10^{-6}\,\frac{d_{\mathrm{t}}}{d_{\mathrm{P}}} + 2{\cdot}10^{-5}\right)\left(\frac{\rho_{\mathrm{f}} v_0 d_{\mathrm{P}}}{\eta_{\mathrm{f}}}\right)^2 \quad (3)$$

for *rings*

$$\frac{\eta_{\mathrm{eff}}}{\eta_{\mathrm{f}}} = 1 + \left(0.0815\frac{d_{\mathrm{t}}}{d_{\mathrm{e,HC}}} - 1.088\right)\left(\frac{\rho_{\mathrm{f}} v_0 d_{\mathrm{e,HC}}}{\eta_{\mathrm{f}}}\right)^{0.6} \quad (4)$$

and for *cylinders*

$$\frac{\eta_{\mathrm{eff}}}{\eta_{\mathrm{f}}} = 1 + \left(1.7{\cdot}10^{-5}\frac{d_{\mathrm{t}}}{d_{\mathrm{a}}} - 1.7{\cdot}10^{-5}\right)\left(\frac{\rho_{\mathrm{f}} v_0 d_{\mathrm{a}}}{\eta_{\mathrm{f}}}\right)^2 \quad (5)$$

It has to be stressed that the correlations for the effective viscosities result from empirical fits between model results and velocity measurements. The main physical impact is the increase of viscosity with increasing Reynolds number. It should be the contents of further work to develop a closed set of correlations for different particle shapes and tube to particle diameters. In the mean time, the range of application should not exceed the range of measurements.

The used radial void fraction profiles can be taken from appendix I. It should be mentioned that recent attempts have been published to solve the flow profile in a randomly packed bed of spheres by direct numerical simulation (e.g., Derkx and Dixon [9] and Lauschke et al. [10]). Here the detailed flow field of a specific pellet arrangement in a tube is resolved. But in addition to the numerical effort the question of turbulence modeling in packed beds has not yet been solved satisfactorily.

3. RADIAL HEAT TRANSFER

Heat transfer perpendicular to the main flow direction consists of convective heat transport, radiation and molecular conductivity through gas and pellets. There is a continuing debate in literature whether heat transfer in packed beds should be modeled with radially varying radial conductivity $\lambda_r(r)$ and $T(r = R) = T_{\mathrm{W}}$ or with a constant radial conductivity plus a wall heat transfer coefficient α_{W} (Krischke et al. [11], Vortmeyer and Haidegger [1]). It is generally agreed, however, that at mass flow velocities between 0.1–2 $\mathrm{kg{\cdot}m^{-2}{\cdot}s^{-1}}$ which are typical of most industrial applications both approaches give similar results [4]. Hence, the classical model of effective heat transfer parameters was applied, lumping together the different physical transport mechanisms into an effective heat conductivity and a heat transfer coefficient at the wall. Using a homogenous model, temperature profiles in packings will be described by the energy balance

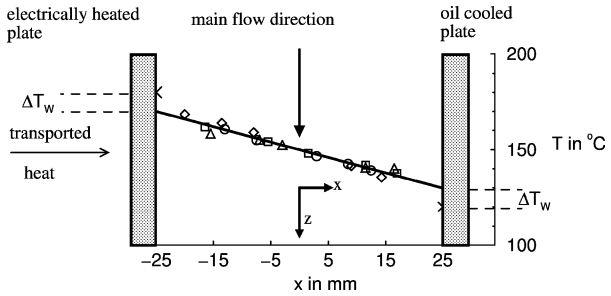

Figure 3. Experimental setup for measuring lateral heat transfer parameters.

$$0 = \dot{m}_{0,z}(r) c_{\mathrm{P}} \frac{\partial T}{\partial z} - \frac{\partial}{\partial z}\left(\lambda_z \frac{\partial T}{\partial z}\right) - \frac{1}{r}\frac{\partial}{\partial r}\left(r\lambda_r \frac{\partial T}{\partial r}\right) \quad (6)$$

Measured radial temperature profiles in packings are characterized by a steep gradient in the vicinity of the wall, which is known to be a consequence of the absence of convective heat transport. The resulting assumption of an unmixed layer at the wall leads to the boundary condition:

$$\lambda_r \left.\frac{\partial T}{\partial r}\right|_{r=R} = \alpha_{\mathrm{W}}\left(T_{\mathrm{W}} - T|_{r=R}\right) \quad (7)$$

For the experimental determination of heat transfer coefficients a setup with a parallel plate geometry was applied (*figure 3*). Comparable setups were used previously by Schroeder et al. [12] to investigate radial heat transfer in water flow through a packed bed. Ofuchi and Kunii [13] used a similar design to determine the stagnant radial heat transfer. But to the best of our knowledge it was the first time a parallel plate geometry was applied to determine the radial heat transfer in gas flow through packed beds.

The two plates were kept at two different temperatures. After an entrance region a linear temperature profile developed in the core of the packing. It was determined by linear regression of the measured temperatures over the width of the packing. The effective heat transfer parameters were obtained directly from the heat flux $\dot{q}_{\mathrm{W}}$ perpendicular to the main flow direction and the temperature gradient or the temperature jump ΔT_{W} at the wall with the following equations:

$$\dot{q}_{\mathrm{W}} = \lambda_r \frac{\mathrm{d}T}{\mathrm{d}x} \quad (8)$$

and

$$\dot{q}_{\mathrm{W}} = \alpha_{\mathrm{W}} \Delta T_{\mathrm{W}} \quad (9)$$

A requirement of the simple evaluation using equations (8) and (9) is that a constant radial temperature profile has been established in the measurement plane. This has been checked by additional temperature measurements as well as by a detailed simulation of axial development of the temperature profile for all experimental conditions used [14].

It should be mentioned that the experiments in the parallel plate apparatus (*figure 3*) yield the effective heat conductivity λ_r and the heat transfer coefficient α_W directly via equations (8) and (9). In contrast, standard experiments in circular tube geometry need to be evaluated by comparison with simulation results using equations (6) and (7). In this evaluation a strong correlation between the λ_r and α_W values obtained cannot be avoided. In addition, the calculated values for the effective heat conductivity λ_r and the heat transfer coefficient at the wall α_W change with the assumed velocity profile which is not the case with the above parallel plate results.

3.1. Determination of heat flux

The configuration of *figure 3* has been realized in a set-up which will briefly be described in the following. More details can be found in [14]. The flow channel was built from two aluminium plates of dimensions given in *figure 4* and from side elements made of teflon for a gap-width of 25 or 50 mm.

One of the aluminium walls was electrically heated by resistance wires the location of which is shown in *figure 4*, left. Around the measurement window additional heating elements are positioned and temperature controlled to the window temperature such that no lateral heat flux would leave or enter the measurement window. At the back side of this plate an oil-heated lid prevented respective heat losses from measurement plane (*figure 4*, right). The electrical heating power applied to the measurement window divided by its area is then the specific heat flux $\dot{q}_W$, required in equations (8) and (9).

The second aluminium wall was thermostated by an oil circuit flowing through slits which were milled into the back of the plate and covered by a lid. The inflow of the oil was inside the measurement window to tightly control its temperature to the set value.

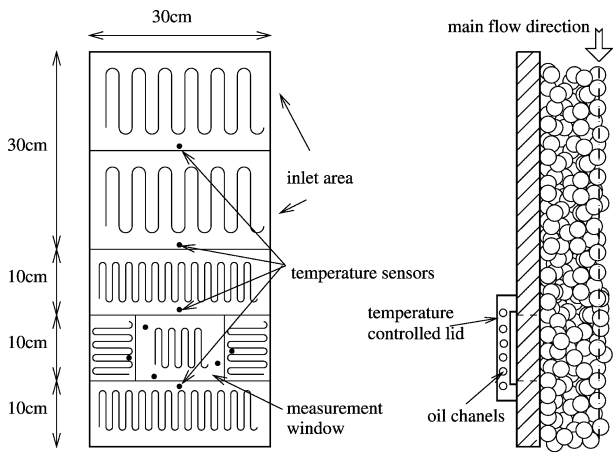

Figure 4. Design of the electrically heated wall (left wall in *figure 3*).

3.2. Determination of the temperature profile in the packing

Sufficiently accurate temperature measurements in a random packing which neither disturb the random nature of the packing nor introduce an additional heat conductivity through the connecting wires present a nontrivial task (Borman et al. [15]). For our set-up the following solution was applied. A fixed random arrangement of pellets for the required gap width was set up by carefully glueing adjacent particles at their contact points together. Into this "particle bridge" arrangement five 0.5 mm OD thermocouples were fixed at specific positions. Four particles bridges were positioned in the measurement window and carefully embedded into the random packing. The thermocouple lets leave the measurement window parallel to the aluminium side walls to prevent any measurement errors due to additional heat conduction.

3.3. Experimental results

Measurements for spheres and rings with different particle diameters have been performed. The geometrical data of the investigated particles are listed in *table I*. Some of the spheres used had an imperfect shape which is typical of industrial catalysts or adsorbents. Three different kinds could be distinguished, ceramic spheres produced by a rolling process, denoted as "spheres, imperfect" with imperfect spherical shape and some variation in mean diameter, spheres from a tabletizing process resembling a flat cylinder with two spherical caps (denoted "spheres, cylindrical") and almost ideal glass spheres.

The values for the effective heat conductivity λ_r could be well described by the correlation of Bauer and Schlünder [16] (see *figure 5*):

TABLE I
Geometrical data of the investigated particles.

Form	Material	d_a [mm]	d_i [mm]	l_P [mm]
sphere, imperfect	ceramic	4.5 ± 2.0	–	–
sphere, cylindrical	ceramic	8.2 ± 0.8	–	–
sphere, imperfect	ceramic	9.8 ± 1.0	–	–
sphere, cylindrical	ceramic	12.0 ± 1.0	–	–
sphere	glass	6.0 ± 0.3	–	–
ring	ceramic	5	2.2	5
ring	ceramic	8	4	8
ring	ceramic	10	5.3	10
ring	ceramic	15	9.5	15

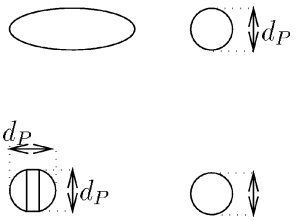

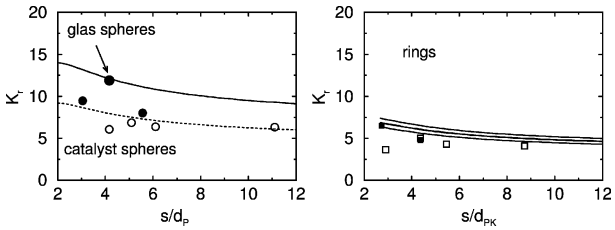

Figure 5. Literature correlations for K_r in a tube and own experimental values for the parallel plate geometry (empty symbols $s = 50$ mm, full symbols $s = 25$ mm).

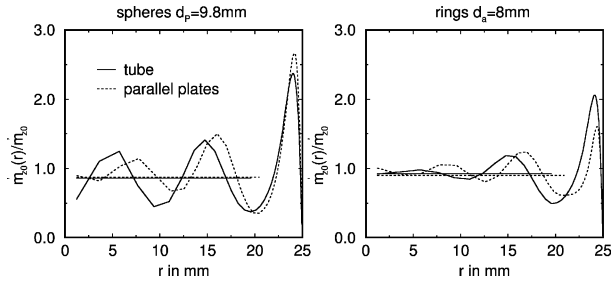

Figure 6. Velocity profiles in round tubes and between parallel plates.

$$\frac{\lambda_r}{\lambda_f} = \frac{\lambda_0}{\lambda_f} + \frac{Pe_P}{K_r} = \frac{\lambda_0}{\lambda_f} + \frac{\dot{m}_0 c_p d_{PS}}{\lambda_f K_r} \quad (10)$$

The heat transfer parameters were determined in two parallel plate slots with a width of $s = 50$ mm and $s = 25$ mm. The measurements in packings of rings and spheres can be correlated with an average error of less than 20 % by the expression

$$Nu_W = 2.4\frac{\lambda_0}{\lambda_f} + 0.065\left(1 - \frac{d_{PS}}{s}\right)^2 Re_P\, Pr^{1/3} \quad (11)$$

Since most technical applications are carried out in round tubes a transformation from the flat geometry to the tube geometry had to be performed. It was based on the assumption that similar flow conditions should lead to similar heat transfer parameters. As characteristic for the wall heat transfer coefficient α_W the maximum velocity close to the wall was considered, the effective radial conductivity was correlated with the velocity in the central part of the packing.

Figure 6 shows the respective flow profiles in a tube and between parallel plates for spheres and rings. It can be seen that in the examples shown the core velocities are almost identical but the peak velocities at the wall differ by a certain amount. To transform the respective Nusselt value measured with the parallel plate velocity profile of *figure 6*, left, to the tube geometry, a different tube velocity (proportional to the differences in the depicted peak velocities) had to be assumed. An experimental verification of this procedure will be presented later.

3.3.1. Effective heat conductivity

The effective heat conductivity is mainly influenced by the velocity in the core of the packing. Hence, the effective heat conductivity was correlated with the mean core velocity (*figure 6*).

Since the core velocities in tube and plate geometry are almost the same, the heat conductivity in packings between parallel plates and in round tubes can be considered identical.

The measured values for the radial heat conductivity λ_r in packings of rings agree well with literature correlations, e.g., Bauer and Schlünder [16] and Dixon [5] (*figures 7* and *8*, right diagrams).

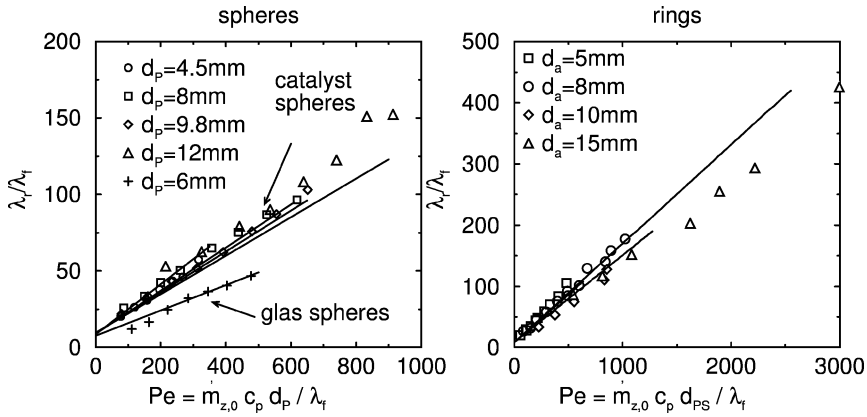

Figure 7. Effective heat conductivities in the tube ($d_t = 50$ mm). The solid lines are represented by equation (12) with $K_{r,t}$ values from *figure 8*.

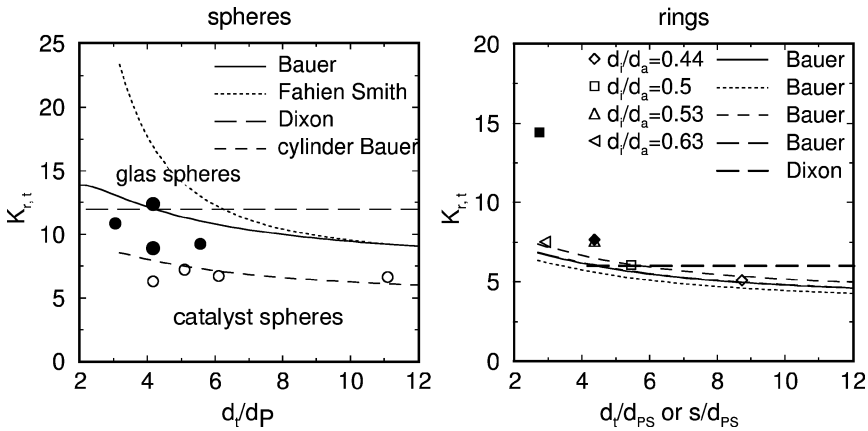

Figure 8. Literature correlations for $K_{r,t}$ and own experimental values (empty symbols $d_t = 50$ mm, full symbols $d_t = 25$ mm).

$$\frac{\lambda_r}{\lambda_f} = \frac{\lambda_0}{\lambda_f} + \frac{\dot{m}_{0,t} c_P d_{PS}}{\lambda_f K_{r,t}} \qquad (12)$$

For catalyst spheres, the measured radial heat conductivities λ_r lie in between the correlations for spheres and for cylinders (*figure 8*). This may be a consequence of the non-ideal shape of the investigated spheres as specified in *table I* and will be taken up later.

3.3.2. Heat transfer coefficient at the wall

The heat transfer parameter at the wall was correlated with the maximum velocity at the wall. The underlying idea consists of the assumption of an unmixed layer at the wall. The thickness of the layer is mainly influenced by the velocity gradient in the vicinity of the wall. The gradient should be described by the maximum velocity.

The wall heat transfer coefficients were correlated as Nusselt numbers $Nu_W = \alpha_W d_P/\lambda_r$ with a linear dependency from Re_P number. As can be seen in *figure 9*, the slope of the Nu_W values decreases with decreasing dimensionless gap width s/d_P.

It is obvious from *figure 9* that for zero flow there is a nonzero wall resistance. This leads to a new correlation for the wall heat transfer coefficient, consisting of a stagnant and a convective term:

$$Nu_W = Nu_{W,0} + a Re_P^m Pr^{1/3} \qquad (13)$$

The stagnant term $Nu_{W,0}$ considers the wall heat transfer resistance at zero flow conditions [17, 18]. Values for $Nu_{W,0}$ have been determined by fitting equation (13) to the measured values in the parallel plate setup. To compare our results with literature correlations $Nu_{W,0}$ was converted into a Biot number by

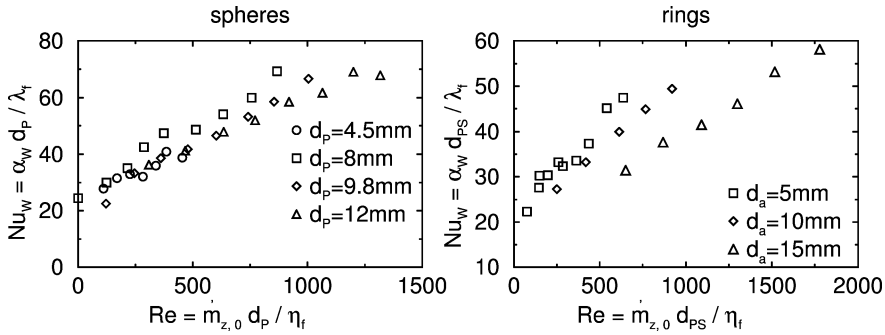

Figure 9. Values for Nu_W over Re measured in the flat setup ($s = 50$ mm).

$$Nu_{W,0} = Bi_0 \frac{\lambda_0}{\lambda_f} 2 \frac{d_P}{d_t} \tag{14}$$

Now these values can be compared with correlations of Nilles [19]

$$Bi_0 2\frac{d_P}{d_t} = \frac{1}{2}\frac{d_t}{d_P}\left(1.3 + 5\frac{d_P}{d_t}\right) \tag{15}$$

or Dixon [5] for spheres

$$Bi_0 2\frac{d_P}{d_t} = 2\frac{d_P}{d_t}\left[2.41 + 0.156\left(\frac{d_t}{d_P} - 1\right)^2\right] \tag{16}$$

and for nonspheres

$$Bi_0 2\frac{d_P}{d_t} = 2\frac{d_P}{d_t}\left[0.48 + 0.192\left(\frac{d_t}{d_P} - 1\right)^2\right] \tag{17}$$

The experimentally obtained values for Bi_0 are in between the different literature correlations but show no significant dependence of the dimensionless tube diameter or the duct width (*figure 10*). A value of $Nu_{W,0} = 2.4\lambda_0/\lambda_f$ was therefore assumed.

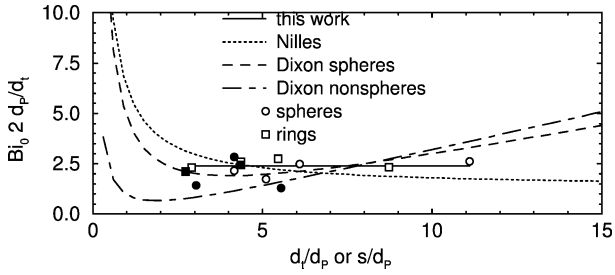

Figure 10. Literature correlations for the Biot number Bi_0 from Nilles [19] and Dixon [5] compared with own measurements in flat channels of $s = 25$ mm (full symbols) and $s = 50$ mm (empty symbols).

The flow contribution of the correlation was fitted to the Reynolds number. The values of Nu_W could be well represented by straight lines, the slope of which decreased with decreasing dimensionless tube diameters d_t/d_P (*figure 11*). The functional dependence on the dimensionless tube diameter, expressed by $(1 - d_P/d_t)$,

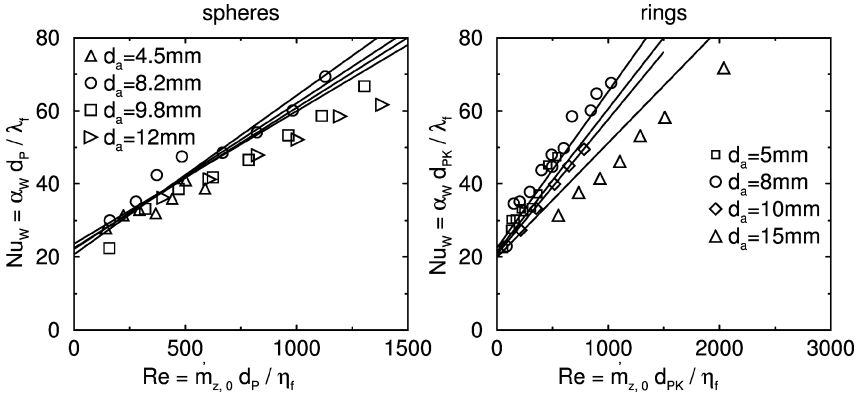

Figure 11. Influence of the particle diameter on the heat transfer coefficient at the wall, α_W, after transformation of the parallel plate measurements ($s = 50$ mm) to the tube ($D = 50$ mm), (—) equation (18).

was taken from the results of Dixon and LaBua [20]. The new correlation based upon the experiments in the flat channels and transformed to round tubes is

$$Nu_W = 2.4\frac{\lambda_0}{\lambda_f} + 0.054\left(1 - \frac{d_{PS}}{d_t}\right) Re_P\, Pr^{1/3} \quad (18)$$

3.3.3. Verification of the heat transfer parameters in the tube

Since the heat transfer experiments for the new correlation, equation (18), have been performed in the parallel plate assembly (*figures 3* and *4*), the correlation has to be verified with experimental data from round tubes. The tube set-up of Daszkowski [21] (see also [2]) was used. A step-change in wall temperature from 20 to 280 °C was applied and the radial temperature profile was determined 40 cm downstream of the wall temperature jump. *Figure 12* shows the measured wall temperatures T_W and the simulated packing temperatures in the tube centre ($r = 0$) and close to the wall ($r = R$). Contrary to previous measurements radial profiles were determined at different angular positions. The results are shown in *figure 13* both as 3D-plot (left) and as radial profiles for different angles (right).

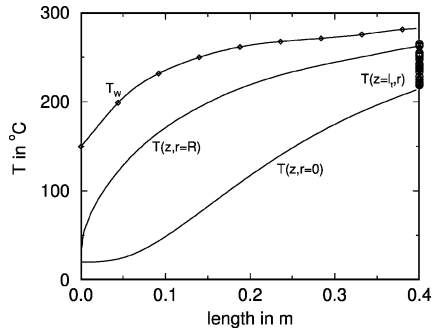

Figure 12. Measured (◊) and simulated axial temperature profiles of the fluid and of the tube wall for the heat-up experiment ($d_P = 4.5$ mm and $\dot{m}_0 = 1.75$ kg·m^{-2}·s^{-1}).

The differences are characteristic of the angular inhomogenity of temperature profiles in packed tubes. As with velocity profiles, careful averaging is necessary to get reliable experimental results.

A quasihomogeneous fixed bed model was used to simulate the heat-up experiment. The axial heat conductivity was calculated after Tsotsas [22]. The flow profile and the radial heat transfer parameters were taken from the above correlations, i.e. the model contained no fitting parameter. The simulation results obtained agree well with the experiments for different spheres and Raschig rings. *Figure 14* shows some examples for catalyst spheres.

For comparison, radial temperature profiles are given using the λ_r-correlation for round spheres of Bauer and Schlünder [16] and the wall heat transfer data of Nilles [19]. In this case a flat (plug flow) velocity profile was assumed as suggested in VDI-Wärmeatlas [22]. The differences are mainly due to differences in $K_{r,t}$ between perfect glass spheres ($K_{r,t} = 12$) assumed by Bauer and Schlünder [16] and nonideal catalyst spheres ($K_{r,t} = 7$) used in this work (see *figure 8*).

4. SUMMARY AND CONCLUSIONS

Velocity profiles below packings of spheres, cylinders and rings were measured. All measured radial flow pro-

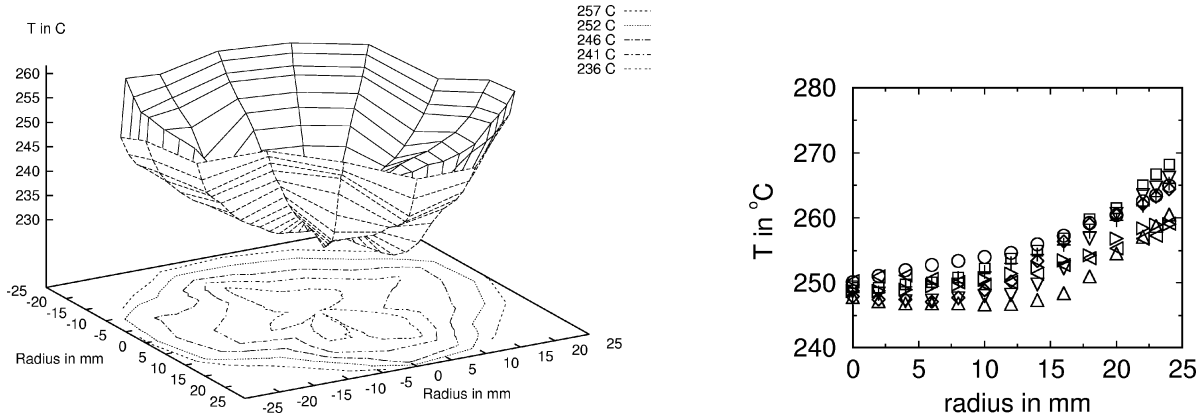

Figure 13. Radial temperature profiles behind a ring packing for the tube heat-up experiment ($d_a = 10$ mm, $\dot{m}_0 = 1.75$ kg·m^{-2}·s^{-1}), left as 3D-plot with isotherm projections, right as radial profiles at different angles in circumferencial direction.

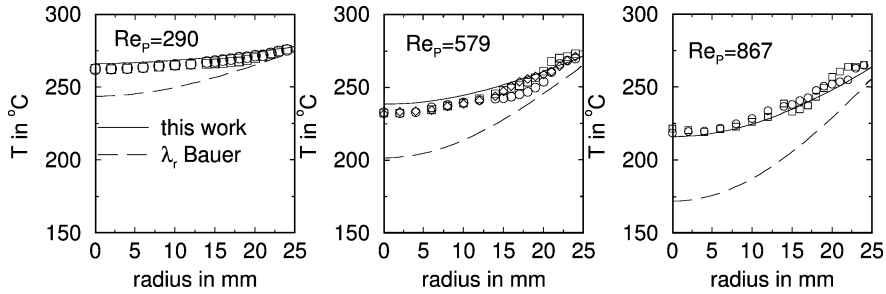

Figure 14. Measured and calculated radial temperature profiles behind a sphere packing ($d_P = 4.5$ mm) for the heat-up experiment. (—) correlation using equation (18), (- - -) using effective heat conductivity λ_r after Bauer and Schlünder [16] for round spheres and heat transfer coefficient at the wall after Nilles [19].

files are characterized by a velocity maximum in the vicinity of the tube wall. Representative flow profiles obtained by averaging the measurements after several repackings were used to determine the influence of the mean velocity and of particle shape and diameter. The flow distribution inside the bed can be described by an extended Brinkman equation. This equation consists of a pressure drop correlation depending on the radially varying void fraction and of a term considering the shear stress in the vicinity of the wall. It turned out that the shear stress at the wall had to be calculated with an "effective turbulent viscosity". Correlations for the effective viscosity based upon the particle Reynolds number have been derived for spheres, rings and cylinder packings. A calculation of radial velocity profiles within random packings of spherical, cylindrical and ring geometry can now be performed using the radial void fraction profiles extracted from literature and the given effective viscosity correlations.

Compared to previous results of Daszkowski and Eigenberger [2] the effective turbulent viscosity reduces the relative velocity maximum close to the wall from a value of $v_{0,\max}/v_0 \approx 4$ to a value of $v_{0,\max}/v_0 \approx 2.5$. This has important implications on the validity of the plug flow assumptions for tubular fixed-bed simulations. Contrary to the findings of Daszkowski and Eigenberger, plug flow seems to be a reasonable assumption for catalytic fixed-bed reactor simulations except for the close vicinity of run-away conditions. This has been shown in a series of simulations in [14]. On the other hand, breakthrough curves of fixed-bed adsorbers are strongly effected by the radially varying velocity profile also if the reduced velocity maximum at the wall is assumed (see [14, 23]).

Detailed radial heat transfer experiments have been performed for a fixed bed between parallel plates. The results allow for the first time determination of lateral heat conductivity and wall heat transfer coefficients for gases independently from each other and independent from the assumptions of an underlying model. The results from parallel plate assembly were transformed to the case of a tube with circular cross section by considering similar flow conditions. This transformation was verified by tube experiments with wall temperature jump. The results are in general agreement with previously published results of Bauer and Schlünder [16], Dixon [5] and Nilles [19]. In particular, the lateral heat conductivity correlations of Bauer and Schlünder [16] could be well confirmed. One notable difference was that catalyst spheres with imperfect shape which are common in industry are better characterized by the radial conductivity of cylinders than of perfect spheres.

For the wall heat transfer coefficient a new correlation (equation (18)) was derived which is valid for use with the radially varying flow profile.

Acknowledgement

The authors gratefully acknowledge the support received for this AiF-project Nr. 9281 from the Minister of Economics of the Federal Republic of Germany. A report (in German) is available from the authors upon request.

REFERENCES

[1] Vortmeyer D., Haidegger E., Discrimination of three approaches to evaluate heat fluxes for wall cooled fixed bed chemical reactors, Chemical Engineering Science 46 (10) (1991) 2651–2660.

[2] Daszkowski T., Eigenberger, G., A reevaluation of fluid flow, heat transfer and chemical reaction in catalyst filled tubes, Chemical Engineering Science 47 (9–11) (1992) 2245–2250.

[3] Papageorgiou J.N., Froment G.F., Simulation models accounting for radial voidage profiles in fixed-bed reactors, Chemical Engineering Science 50 (19) (1995) 3043–3056.

[4] Tsotsas E., Über die Wärme- und Stoffübertragung in durchströmten Festbetten, VDI-Fortschrittsberichte, Reihe 3: Verfahrenstechnik Nr. 223, VDI-Verlag, Düsseldorf, 1990.

[5] Dixon A.G., Wall and particle-shape effects on heat transfer in packed beds, Chem. Engrg. Comm. 71 (1988) 217–237.

[6] Bey O., Eigenberger G., Fluid flow through catalyst filled tubes, Chemical Engineering Science 52 (8) (1997) 1365–1376.

[7] Borkink J.G.H., Heat transport in wall-cooled packed beds of low tube-to-particle diameter ratio, Ph.D. Thesis, University Twente, 1991.

[8] Giese M., Rottschäfer K., Vortmeyer D., Measured and modelled superficial flow profiles in packed beds with liquid flow, AIChE J. 44 (1998) 484–490.

[9] Derkx O.R., Dixon A.G., Determination of the fixed bed wall heat transfer coefficient using computational fluid dynamics, Numer. Heat Tran. A 29 (1996) 777–794.

[10] Lauschke G., Brander B., Drews A., Clarkson R., Haimad N., A model for three-dimensional simulation of catalytic packed bed reactors using CFD, in: International Symposium on Chemical Reaction Engineering, 15th ISCRE, 1998.

[11] Krischke A., Winterberg M., Tsotsas E., Vortmeyer D., Wärmetransport und chemische Reaktion in durchströmten Festbetten — eine Neuevaluierung, in: GVC-Jahrestagung, 1998.

[12] Schroeder K.J., Renz U., Elgeti K., Forschungsberichte des Landes Nordrhein-Westfalen Nr. 3037, 43 (9) (1981) 2523–2532.

[13] Ofuchi K., Kunii D., Heat transfer characteristics of packed beds with stagnant fluids, Trans. ASME, J. Heat Mass Tran. 8 (1965) 749–757.

[14] Bey O., Strömungsverteilung und Wärmetransport in Schüttungen VDI-Fortschrittsberichte, Reihe 3: Verfahrenstechnik Nr. 570, VDI-Verlag, Düsseldorf, 1998.

[15] Borman P.C., Borkink J.G.H., Westerterp K.R., Heat transport in a wall heated tubular packed bed reactor at elevated pressures and temperatures, Chem. Engrg. Comm. 114 (1992) 17–47.

[16] Bauer R., Schlünder E.U., Die effektive radiale Wärmeleitfähigkeit gasdurchströmter Schüttungen, Verfahrenstechnik 11 (10) (1977) 605–613.

[17] Dixon A.G., Cresswell D.L., Theoretical prediction of effective heat transfer parameters in packed beds, AIChE J. 25 (4) (1979) 663–676.

[18] Dixon A.G., Heat transfer in fixed beds at very low (< 4) tube-to-particle diameter ratio, Ind. Eng. Chem. Research 36 (8) (1997) 3053–3064.

[19] Nilles M., Wärmeübergang an der Wand durchströmter Schüttungsrohre, VDI-Forschungsberichte, Reihe 3: Verfahrenstechnik Nr. 264, VDI-Verlag, Düsseldorf, 1991.

[20] Dixon A.G., LaBua L.A., Technical notes: Wall-to-fluid coefficients for fixed bed heat and mass transfer, Int. J. Heat Mass Tran. 28 (4) (1985) 879–881.

[21] Daszkowski T., Strömung, Stoff- und Wärmetransport in schüttungsgefüllten Rohrreaktoren, Ph.D. Thesis, Institut für Chemische Verfahrenstechnik, Universität Stuttgart, 1991.

[22] Tsotsas E., Wärmeleitung und Dispersion in durchströmten Schüttungen, in: VDI-Wärmeatlas, 8 edition, Verein Deutscher Ingenieure, 1997.

[23] Boger T., Einsatz von Zeolithen und MC-41-Materialien zur adsorptiven Abtrennung aromatischer Kohlenwasserstoffe, Ph.D. Thesis, Institut für Chemische Verfahrenstechnik, Universität Stuttgart, 1999.

[24] Brauer H., Grundlagen der Einphasen- und Mehrphasenströmungen, Verlag Sauerländer, Aarau/Frankfurt am Main, 1971.

[25] Dixon A.G., Correlations for wall and particle shape effects on fixed bed bulk voidage, Can. J. Chem. Eng. 66 (1988) 705–708.

[26] Brauer H., Druckverlust in Füllkörpersäulen bei Einphasenströmung, Chem.-Ing.-Techn. 29 (12) (1957) 785–790.

APPENDIX I

Radial void fraction profiles in tubes

The following correlations are described in detail in [6]. They were extracted from literature measurements. The geometrical data of the particles used are shown in *table II*.

For *spheres* the voidage profiles can be described by

$$x_{\min} = 0.5\left(d_t - \sqrt{(d_t - d_P)^2 - d_P^2}\right)$$

$$r' = \frac{d_t/2 - r}{x_{\min}} - 1$$

$$\varepsilon_{\text{wall}} = \varepsilon_{\min} + (1 - \varepsilon_{\min})\left(r'\right)^2 \quad \text{for } r' < 0$$

$$\varepsilon_{\text{core}} = \varepsilon_0 + (\varepsilon_{\min} - \varepsilon_0)\exp\left(-\frac{r'}{c}\right)\cos\left(\frac{\pi}{b}r'\right) \quad \text{for } r' \geq 0 \tag{I.1}$$

with

$$\varepsilon_{\min} = 0.24 \tag{I.2}$$

$$b = 0.876 \tag{I.3}$$

$$c = 10 \tag{I.4}$$

ε_0 was adjusted by fitting the integrated profile of $\varepsilon(r)$ (equation I.1) to the value of $\overline{\varepsilon}_S$ obtained by an empirical correlation of Jeshar [24] for the voidage of the whole cross section $\overline{\varepsilon}_S$:

$$\overline{\varepsilon}_S = 0.375 + 0.34\frac{d_P}{d_t} \tag{I.5}$$

The correlation of the void fraction profile in packings of *cylinders* is similar to the correlation for spheres:

TABLE II
Geometrical data of the investigated particles.

Shape	d_a [mm]	d_i [mm]	l_P [mm]	ε_{min}	ε_0	$\frac{2}{R^2}\int r\varepsilon(r)\,dr$	$\overline{\varepsilon}$
							equation (I.5):
sphere	4.5 ± 2.0	–	–	0.27	0.39	0.409	0.406
sphere	6.3 ± 1.0	–	–	0.24	0.39	0.418	0.418
sphere	7.5 ± 1.0	–	–	0.24	0.395	0.427	0.426
sphere	9.8 ± 1.0	–	–	0.24	0.41	0.448	0.442
sphere	14 ± 1.5	–	–	0.24	0.41	0.47	0.47
							equation (I.9):
cylinder	4.5	–	4.5	0.275	0.365	0.377	0.378
cylinder	6	–	6	0.275	0.375	0.389	0.387
cylinder	12	–	12	0.3	0.42	0.44	0.44
cylinder	6	–	5–20	0.275	0.365	0.38	0.378
							equation (I.11):
ring	5	2.2	5.5	0.38	0.476	0.50	0.50
ring	8	4	8	0.42	0.513	0.55	0.55
ring	10	5.3	10	0.45	0.533	0.587	0.583
ring	15	9.5	15	0.545	0.613	0.689	0.687

$$r' = a_0 \frac{R - r}{d_a} - 1$$

$$a_0 = 1.8 - 2\frac{d_P}{d_R}$$

$$\varepsilon_{wall} = \varepsilon_{min,C} + (1 - \varepsilon_{min,C})\left(r'\right)^4 \quad \text{for } r' < 0$$

$$\varepsilon_{core} = \varepsilon_{0,C} + (\varepsilon_{min,C} - \varepsilon_{0,C}) \exp\left(-\frac{r'}{c}\right) \cos\left(\frac{\pi}{b} r'\right)$$

$$\text{for } r' \geq 0 \qquad \text{(I.6)}$$

with

$$b = 0.876 \qquad \text{(I.7)}$$

$$c = 2 \qquad \text{(I.8)}$$

The data for ε_0 were again developed from correlations for $\overline{\varepsilon}$ [25]:

$$\overline{\varepsilon}_C = 0.36 + 0.1\frac{d_{PS}}{d_t} + 0.7\left(\frac{d_{PS}}{d_t}\right)^2 \quad \text{for } \frac{d_{PS}}{d_t} \leq 0.6 \qquad \text{(I.9)}$$

Voidage profiles for *rings* were calculated by

$$r' = a_0 \frac{R - r}{d_a} - 1$$

$$a_0 = 1.8 - 2\frac{d_a}{d_t}$$

$$\varepsilon_{wall} = \varepsilon_{min,HC} - (1 - \varepsilon_{min,HC})\left(r'\right)^2 \quad \text{for } r' < 0$$

$$\varepsilon_{core} = \varepsilon_{0,HC} + (\varepsilon_{min,HC} - \varepsilon_{0,C})\, e^{-r'/c} \cos\left(\frac{\pi r'}{0.876}\right)$$

$$\text{for } r' \geq 0 \qquad \text{(I.10)}$$

The mean void fraction for rings of the whole cross section $\overline{\varepsilon}_{HC}$ with $d_i/d_a < 0.5$ results directly from the void fraction distribution of full cylinders as shown by Dixon [25]):

$$\overline{\varepsilon}_{HC} = \overline{\varepsilon}_C + (1 - \varepsilon_i)\overline{\varepsilon}_C \qquad \text{(I.11)}$$

To avoid identical values for $\varepsilon_{0,HC}$ and $\varepsilon_{min,HC}$, a packing of cylinders with $\varepsilon_{0,HC} = 0.35$ and $\varepsilon_{min,C} = 0.23$ was fixed as the origin of the voidage profiles for the rings. Assuming the inner void fraction of the rings distributed evenly over the radius as described in equation (I.10), the data for $\varepsilon_{0,HC}$ and $\varepsilon_{min,C}$ can be obtained from

$$\varepsilon_{0,HC} = \varepsilon_i + \varepsilon_{0,C}(1 - \varepsilon_i) \qquad \text{(I.12)}$$

$$\varepsilon_{min,HC} = \varepsilon_i + \varepsilon_{min,C}(1 - \varepsilon_i) \qquad \text{(I.13)}$$

APPENDIX II

Equations to evaluate lateral velocity profiles

To evaluate axially developed lateral velocity profiles in setups with parallel plate geometry, a momentum

balance, correlations for effective viscosities and for lateral void fraction profile are used. Details can be drawn from Bey [14].

Momentum balance in the flat duct

$$\frac{\mathrm{d}p}{\mathrm{d}z} = -150\eta_\mathrm{f}\frac{(1-\varepsilon(x))^2}{\varepsilon(x)^2 d_\mathrm{e}^2}v(x) - 1.75\rho_\mathrm{f}\frac{(1-\varepsilon(x))}{\varepsilon(x)d_\mathrm{e}}v(x)^2 + \frac{\eta_\mathrm{eff}}{\varepsilon(x)}\frac{\mathrm{d}}{\mathrm{d}x}\left(\varepsilon(x)\frac{\mathrm{d}v(x)}{\mathrm{d}x}\right) \quad \text{(II.1)}$$

Boundary condition:

$$v_{0,z} = \frac{1}{s}\int_0^s v(x)\varepsilon(x)\,\mathrm{d}x \quad \text{(II.2)}$$

For hollow cylinders the hydrodynamic diameter after Brauer [26] is used:

$$d_\mathrm{e,HC} = \frac{6}{a_\mathrm{spec}}\left(\frac{1-\varepsilon_\mathrm{i}}{1+(2/3)\sqrt{\varepsilon_\mathrm{i}}-\varepsilon_\mathrm{i}/3}\right)^n = \frac{6}{a_\mathrm{spec}}E^n \quad \text{(II.3)}$$

The exponent $n = 1.9$ weights the inner void fraction of the rings.

The fitted values for the effective viscosities can be correlated for spheres by

$$\frac{\eta_\mathrm{eff}}{\eta_\mathrm{f}} = 1 + \left(6.42{\cdot}10^{-6}\frac{s}{d_\mathrm{P}} - 1.37{\cdot}10^{-5}\right)\left(\frac{\rho_\mathrm{f}v_0 d_\mathrm{P}}{\eta_\mathrm{f}}\right)^2 \quad \text{(II.4)}$$

for rings by

$$\frac{\eta_\mathrm{eff}}{\eta_\mathrm{f}} = 1 + 2.75{\cdot}10^{-5}\left(\frac{s}{d_\mathrm{e,HC}}\right)^2\left(\frac{\rho_\mathrm{f}v_0 d_\mathrm{e,HC}}{\eta_\mathrm{f}}\right)^{1.2} \quad \text{(II.5)}$$

Lateral void fraction profiles between parallel plates

Because no measurements of lateral voidage profiles in literature are known, a simple experimental setup was used. The space between two parallel plates was filled with particles. The voidage between the particles was filled with silicon oil step by step. From the fluid volume and the total volume, the local voidage can be determined. The geometrical data of the investigated particles are shown in *table III*.

TABLE III
Geometrical data of the investigated particles in the flat duct.

Form	d_a [mm]	d_i [mm]	l_P [mm]	ε_min	ε_0	$\overline{\varepsilon}$
sphere	4.5 ± 2.0	–	–	0.27	0.39	0.401
sphere	9.8 ± 1.0	–	–	0.24	0.41	0.424
ring	5	2.2	5.5	0.436	0.538	0.547
ring	8	4	8	0.475	0.57	0.584
ring	10	5.3	10	0.5	0.588	0.594
ring	15	9.5	15	0.58	0.657	0.683

For spheres the measurements can be described with the following correlation:

$$x' = \frac{2(s/2-x)}{d_\mathrm{P}} - 1$$
$$\varepsilon_\mathrm{wall} = \varepsilon_\mathrm{min} + (1-\varepsilon_\mathrm{min})\left(x'\right)^2 \quad \text{for } x' < 0$$
$$\varepsilon_\mathrm{core} = \varepsilon_0 + (\varepsilon_\mathrm{min}-\varepsilon_0)\exp\left(-\frac{x'}{c}\right)\cos\left(\frac{\pi}{b}x'\right) \quad \text{for } x' \geq 0 \quad \text{(II.6)}$$

with $b = 0.876$ and $c = 2$.

For rings the following correlation was used:

$$x' = a_0\frac{s/2-x}{d_\mathrm{a}} - 1$$
$$a_0 = 2 - 1.5\frac{d_\mathrm{a}}{s}$$
$$\varepsilon_\mathrm{wall} = \varepsilon_\mathrm{min} - (1-\varepsilon_\mathrm{min})\left(-x'\right)^3 \quad \text{for } x' < 0$$
$$\varepsilon_\mathrm{core} = \varepsilon_0 + (\varepsilon_\mathrm{min}-\varepsilon_0)\,\mathrm{e}^{-x'/c}\cos\left(\pi x'\right) \quad \text{for } x' \geq 0 \quad \text{(II.7)}$$

with $c = 2$, $b = 1$, $\varepsilon_\mathrm{min,C} = 0.3$ and $\varepsilon_\mathrm{0,C} = 0.427$:

$$\varepsilon_\mathrm{0,HC} = \varepsilon_\mathrm{i} + \varepsilon_\mathrm{0,C}(1-\varepsilon_\mathrm{i}) \quad \text{(II.8)}$$
$$\varepsilon_\mathrm{min,HC} = \varepsilon_\mathrm{i} + \varepsilon_\mathrm{min,C}(1-\varepsilon_\mathrm{i}) \quad \text{(II.9)}$$